Applied Surface Science 255 (2008) 2646–2650

Contents lists available at ScienceDirect

Applied Surface Science

journal homepage: www.elsevier.com/locate/apsusc

# Low-temperature growth and optical properties of Ce-doped ZnO nanorods

Jinghai Yang [a,b,*], Ming Gao [a], Lili Yang [a], Yongjun Zhang [a], Jihui Lang [a], Dandan Wang [b], Yaxin Wang [a], Huilian Liu [a,b], Hougang Fan [a]

[a] The Institute of Condensed State Physics, Jilin Normal University, Siping 136000, People's Republic of China
[b] Key Laboratory of Excited State Processes, Changchun Institute of Optics, Fine Mechanics and Physics, Chinese Academy of Sciences, Changchun 130033, People's Republic of China

ARTICLE INFO

*Article history:*
Received 13 October 2007
Received in revised form 30 June 2008
Accepted 2 August 2008
Available online 6 August 2008

*PACS:*
71.55.Gs
78.55.−m
78.67.−n

*Keywords:*
Ce-doped ZnO nanorods
Sol–gel
Optical properties

ABSTRACT

Ce-doped ZnO nanorods were prepared by sol–gel method with low annealing temperature of 500 °C. The effects of Ce doping on the structural and optical properties of ZnO nanorods were investigated in detail. The samples were characterized by X-ray diffraction (XRD), scanning electron microscopy (SEM), X-ray photoelectron spectroscopy (XPS), photoluminescence (PL) and Raman-scattering spectroscopy measurements. The XRD results showed that Ce was doped into ZnO nanorods because of no diffraction peaks of Ce or cerium oxide in the pattern. The synthesis temperature of Ce-doped ZnO nanorods decreased from 900 to 500 °C compared to that of pure ZnO nanorods. Compared with pure ZnO, UV peaks shifted towards the blue color and the intensity of visible peaks decreased after Ce doping. The PL properties of Ce-doped ZnO nanorods depend on both the synthesis temperatures and the dopant. In Raman spectra of doped samples, some classical modes, such as $A_1$ and $E_1$ modes, disappear, and the $E_2$ modes blue shift.



## 1. Introduction

Among numerous semiconductor nanomaterials, ZnO nanorods are attractive components for nanometer-scale electronic and photonic device applications [1–3]. Recently, ZnO nanorods are utilized to fabricate various nanodevices including ultraviolet photodetectors, Schottky diodes, and light emitting diode arrays [4–6]. On the basis of the controllable synthesis of pure phase nanorods, doping with selective elements offers an effective method to adjust the electrical, optical, and magnetic properties of ZnO, which is crucial for its practical application. ZnO was frequently doped with group III, IV, V, and VI elements (e.g., Al, Ga, In, Sn, Sb and S) [7]. Due to its potential optoelectronic applications, nowadays the rare earth (RE, e.g., Eu, Tb, Er, Tm) [8–11] doped ZnO is an interesting field of study. Part of this interest lies in the shielded 4f levels of $RE^{3+}$, which can make various well-defined narrow optical transitions happen between the spin orbit levels split under the different manifolds weak crystal field. Cerium is a major element in the useful rare earth family. Up to now, there was limited reports about fabrication of Ce-doped ZnO nanostructures [12,13]. Moreover, the dopant sites, defects induced by the doping and especially the possible host electronic structure change upon doping have strong impacts on the optical properties of these nanorods. As far as we known, little has been investigated when rare earth (such as Ce) was doped into ZnO nanorods. So the structures, optical and electrical properties of Ce-doped ZnO nanorods still need further research, which is very important for both fundamental and applied points of view.

Sol–gel method is easily reproducible and applicable to large industrial scale fabrication of products at low cost. Recently, the growth temperature with sol–gel technique of ZnO nanorods are above 900 °C. Ce-doped 1D ZnO nanostructures synthesized by sol–gel processing were still 850 °C [12]. Such higher temperature makes it difficult to fabricate samples on the low-cost flexible substrates. In this paper, Ce-doped ZnO nanorods were synthesized under low temperature of 500 °C by sol–gel method, which provides a promising option for large-scale productions of Ce-doped ZnO nanorods. The effects of cerium doping on the structural and optical properties of ZnO nanorods were also investigated in detail.

* Corresponding author at: The Institute of Condensed State Physics, Jilin Normal University, Siping 136000, People's Republic of China. Tel.: +86 434 3290009; fax: +86 434 3294566.
*E-mail address:* jhyang@jlnu.edu.cn (J. Yang).

0169-4332/$ – see front matter © 2008 Elsevier B.V. All rights reserved.
doi:10.1016/j.apsusc.2008.08.001

## 2. Experimental

Pure ZnO nanorods and Ce-doped ZnO nanorods were prepared in this experiment. The concentration of Zinc nitrate hexahydrate and citric acid were fixed on 0.01 M in the reaction. The mixed solution was stirred for 2 h, and then kept in the drying cabinet for some hours to form dried gel. The dried gel was kept in the box furnace at 400 °C for 1 h to get amorphous precursor of Zn–C–O composite powders. Then this precursor was sintered under 900 °C for 13 h. Finally the white powders were obtained after cooling down to room temperature. For Ce-doped ZnO nanorods, the solution of cerium nitrate hexahydrate was fixed on 0.0002 M and zinc nitrate hexahydrate was 0.0098 M. In addition, 0.04 M ethylene glycol was added into the chemical solution to produce ZnO nanostructures. The same drying process was followed as mentioned previously. The dried gel was sintered at 500 °C for 6 h to get Ce-doped ZnO nanorods.

X-ray diffraction (XRD) (MAC Science, MXP18, Japan), scanning electron microscopy (SEM) (Hitachi, S-570), X-ray photoelectron spectroscopy (XPS) (VG ESCALAB Mark II), photoluminescence (PL) (He–Cd Laser, 325 nm) and Raman spectroscopy (514.5 nm, argon ion laser, Labram-HR) were used to characterize the crystal structure, surface morphology and optical properties of ZnO nanorods.

## 3. Experimental results and discussion

Fig. 1 shows XRD patterns of as-prepared ZnO and Ce-doped ZnO samples. The diffraction peaks in the XRD spectra indicated that the both samples had typical hexagonal wurtzite structures. For Ce-doped ZnO, no diffraction peaks of Ce or other impurity phases were found in our samples, suggesting that $Ce^{3+}$ ions would uniformly substitute into the $Zn^{2+}$ sites or interstitial sites in ZnO lattice. Moreover, the major diffraction peaks shift slightly towards smaller diffraction angle compared to the standard card (JCPDS 79-2205, $a$ = 3.250 and $c$ = 5.207). The lattice parameter $c$ calculated from the (0 0 2) peak of Ce-doped ZnO sample is 5.284 nm. The increase of lattice constant suggested that the larger $Ce^{3+}$ substitutes the smaller $Zn^{2+}$ site partly so that the lattice constant increased. In addition, the peak intensity decreases greatly and the width broadens which implied that $Ce^{3+}$-doped 1D ZnO nanorods with a smaller average diameter was synthesized.

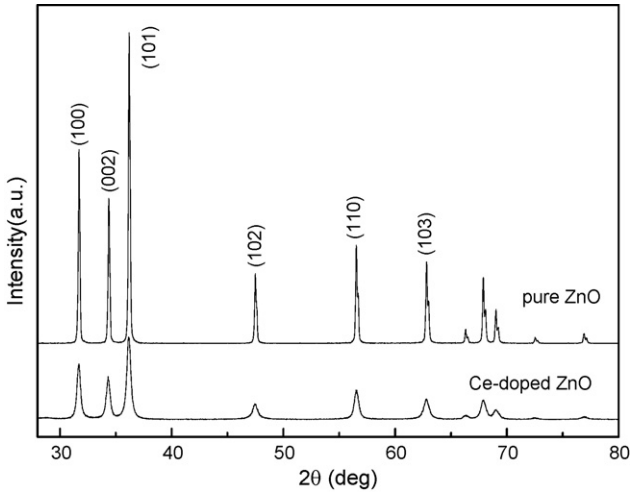


**Fig. 1.** XRD spectra of Ce-doped and undoped ZnO samples.

The morphology and microstructure of the as-grown materials were characterized and analyzed by SEM. SEM image (Fig. 2a) showed that the as-grown products prepared by sintering at 900 °C have a uniform size and rod like shape with average diameter of about 300 nm and length up to about 1–3 μm. When the sintering temperature was below 900 °C, no ZnO nanorod can be found in the undoped sample. Good quality Ce-doped ZnO nanorods can be obtained at 500 °C, and the lengths of the nanorods reach several micrometers and the diameters range from 100 to 200 nm in Fig. 2b. SEM results has good agreement with XRD results discussed before.

Ce may be an ideal material to be doped into ZnO nanorods due to the similar lattice constant. So we proposed a possible mechanism for the growth of Ce-doped ZnO nanorods at low temperature. This can be attributed to a preferential transformation of $Ce^{3+}$ ions. $CeO_2$ fine nanocrystals were first formed in the Ce–Zn complex sol–gel system after annealing at 500 °C. These nanocrystals have many different crystal faces with different surface energy. It is well known that an impetus for aggregation of nanoparticlesis is to reduce surface energy by eliminating the higher surface energy face. Some of crystal faces could well reduce the surface energy of ZnO, and nanocrystalline can be formed quickly under the condition of low temperature. The Ce–Zn

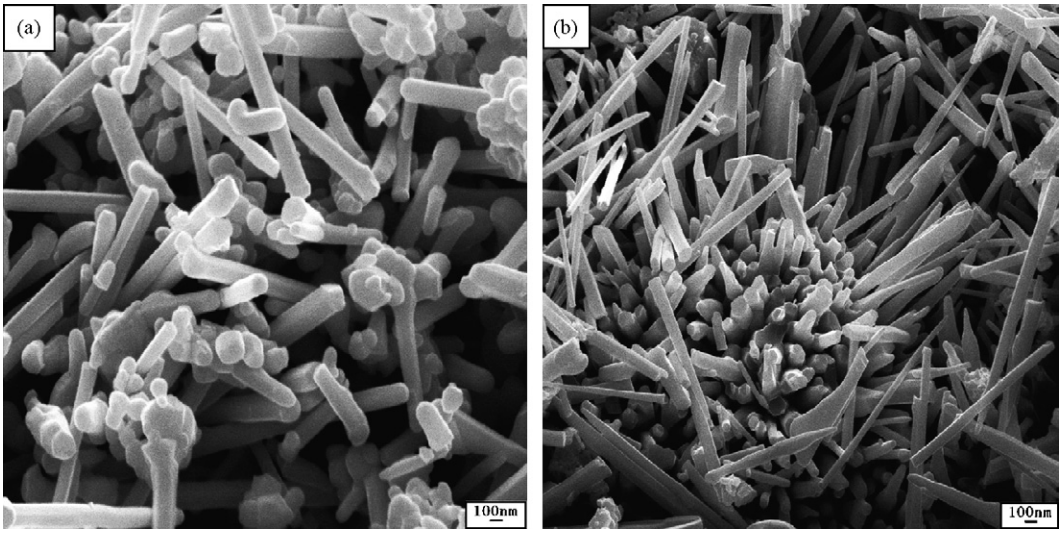


**Fig. 2.** SEM of the undoped ZnO (a) and Ce-doped ZnO (b).

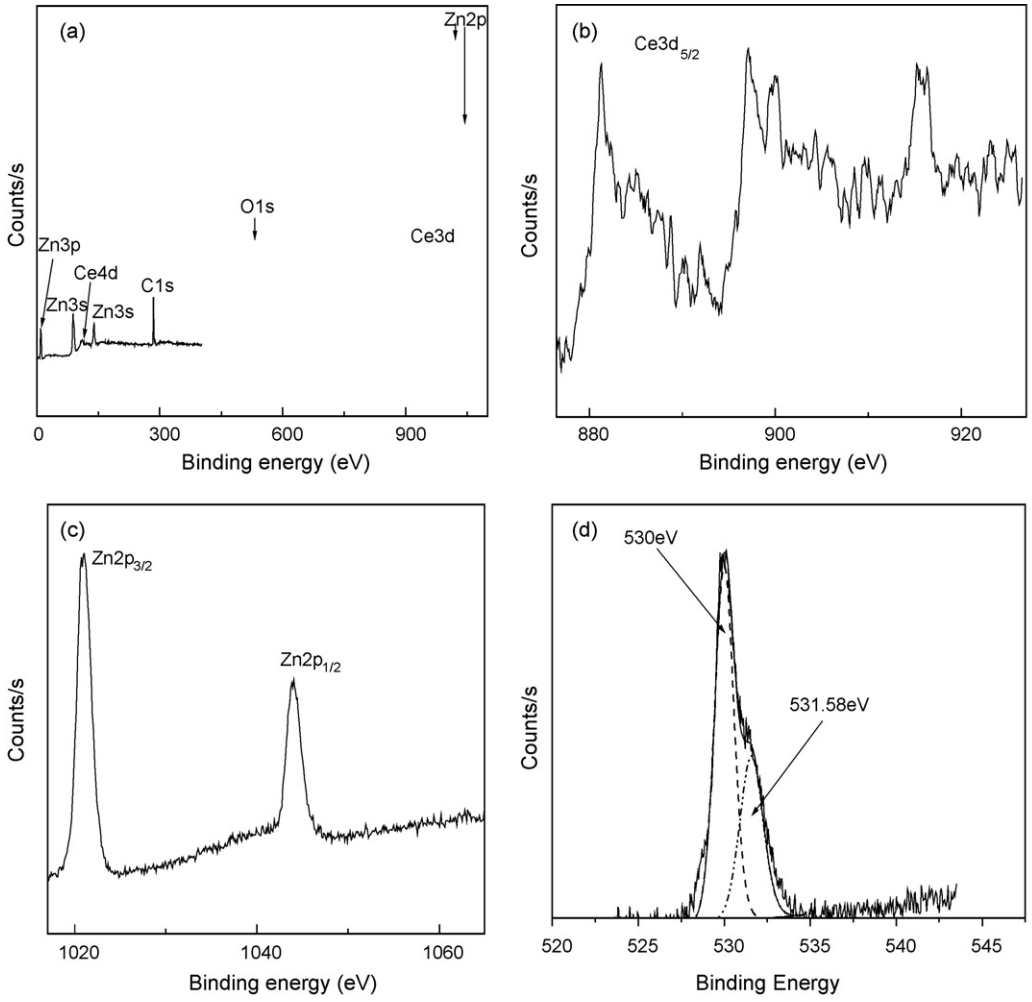


**Fig. 3.** XPS spectrum of the Ce-doped ZnO nanorods annealed at 500 °C. (a)–(d) Showed the high resolution scans of Ce 3d, Zn 2p and O 1s.

complex sol–gel system further crystallized along these crystal faces to form the final morphology of 1D nanorods. Further investigations are still need to better understand the formation of Ce-doped ZnO nanorods.

The incorporation mode of Ce ions in the ZnO lattice and their vibration states were characterized by XPS measurement. Fig. 3a shows the typical XPS spectra of the Ce-doped ZnO nanorods annealed at 500 °C. The high resolution scans of Ce 3d, Zn 2p and O 1s shown in Fig. 3b–d. The peaks located at 1021 and 1044 eV correspond to Zn $2p_{3/2}$ and Zn $2p_{1/2}$, respectively. The high-resolution scans also showed that the binding energy of Ce $3d_{5/2}$ located at 881.3, 897.1 and 915.3 eV and O 1s at 530.1 eV. Compared with standard XPS energy peak location of Ce $3d_{5/2}$ at 884.9, 898.2 and 915.7 eV, the peaks Ce $3d_{5/2}$ for the Ce-doped ZnO nanorods have a slightly blue shift, indicating that the distance between Ce and O in $Ce_2O_3$ has changed due to $Ce^{3+}$ ions doped into ZnO lattices, which is similar to ZnO:Tb thin films [9]. In the O 1s region, there are two distinct components to the observed peak shape: an intense low-energy component at 530 eV and a high-energy component at 531.58 eV. Brundle et al. reported the former is associated with photoemission in $O^{2-}$ ions with valence state comparable to that of oxygen found in a bulk ZnO crystal; the latter is associated with a lower oxygen valence, e.g., $O^{-}$ [14].

Fig. 4a shows the PL spectra of the ZnO and Fig. 4b shows the PL spectra of the Ce-doped ZnO nanorods excited by 325 nm at room temperature. The PL spectra of ZnO nanorods contain a strong UV band peak at 390 nm. Besides, a relatively strong and broad green band centered at about 513 nm occurred. The UV emission is originated from excitonic recombination corresponding to the near-band-edge emission of ZnO. The green emission peak is commonly

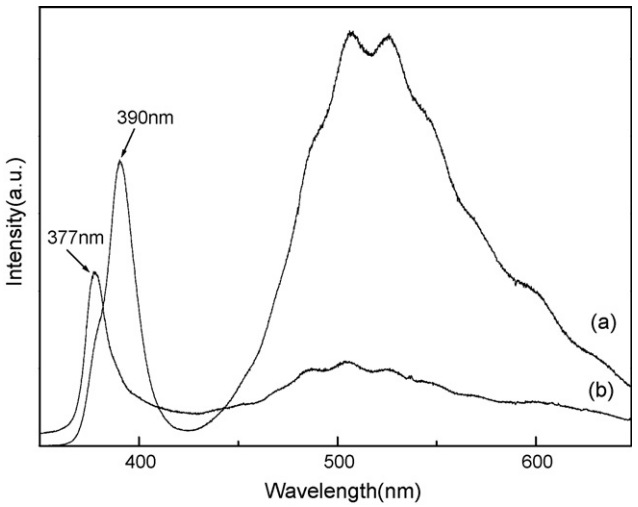


**Fig. 4.** PL of undoped ZnO nanorods prepared at 900 °C (a) and prepared with Ce-doping nanorods at 500 °C (b).

referred to deep-level or trap-state emission [15,16]. Various mechanisms have been proposed for the visible light emission of ZnO. Oxygen vacancies occur in three different charge states: the neutral oxygen vacancy ($V_O$), the singly ionized oxygen vacancy ($V_O^{\bullet}$), and the doubly ionized oxygen vacancy ($V_O^{\bullet\bullet}$) [17]. Vanheusden et al. found that only the singly ionized oxygen vacancies ($V_O^{\bullet}$) are responsible for the green luminescence in the ZnO [18]. Compared with the PL spectrum of ZnO nanorods, the peak position of Ce-doped ZnO nanorods UV emission exhibits large blue shift while the green emission band is sharply suppressed. For Ce-doped ZnO nanorods, more electrons contributed by cerium dopants would take up the energy levels located at the bottom of conduction band. When they were excited by the laser of 325 nm, the excitons take up higher-energy levels at the bottom of conduction band. Radioactive recombination of these excitons will lead to a blue shift and broaden of UV emission peak [19]. The lattice strain induced by the lattice distance would also lead to some shift in band gap but may not play a major role in the determination of band gap as the small deformation of the lattice distances. Decreased UV emission was considered due to the increase of the nanoradiative defects and decrease of ZnO nanorod size [20]. A blue shift of the band edge revealed from PL points to the incorporation of at least a part of Ce on the lattice sites. This supports the X-ray results on the incorporation of Ce into the nanorod structure. The spectra showed that the intensities of the green peak were sharply suppressed both affected by annealing temperature. In comparing Fig. 4a and b, the green emission peak of the Ce-doped ZnO nanorods was sharply suppressed and broadened. We ascribe the decrease of the green emission intensity after cerium doping to the decrease of annealing temperature. When the ZnO are heated, they tend to lose oxygen [21]. Though there was no consensus in the literature on the origin of green emission in ZnO, its intensity was commonly related to the density of intrinsic defects (such as oxygen vacancy or Zn interstitial related defects) [22] and the special surface structure [23,24]. It was believed that the more ZnO nanorods were heated by higher annealing temperature, the more oxygen was lost, increasing the visible luminescence. Although the oxygen vacancy was an intrinsic donor [25] in ZnO, the coexistence of another donor (possibly interstitial Zn) with a much higher density must be considered. Hence, Zn atoms were likely to diffuse into the nanorods in interstitial sites where they acted as shallow donors [26]. In these investigations the decrease of visible luminescence of Ce-doped ZnO nanorods was strongly related to the decreases of oxygen vacancies and interstitial Zn by low-annealing temperature process. When Ce ions are incorporated into ZnO and become donors, multi-emission centers are formed, such as the emission of the electron–hole plasma (EHP), the emission of the donors to the valence band, and the intrinsic transition of $Ce^{3+}$ ions [27]. So the green emission of Ce-doped ZnO nanorods was more broad than the undoped. The PL integrated intensity ratio of the UV emission to the deep-level green emission ($I_{UV}/I_{DLE}$) is 0.69 and 2.06, for ZnO and Ce-doped ZnO nanorods, respectively. Generally, the intensity ratio of UV emission band to visible emission band is regarded as an indicator of the crystal of ZnO materials. The strong UV and weak green bands imply good crystal surface [28]. The increased ratio suggests the good crystal of Ce-doped ZnO nanorods. Our results showed a great promise for the Ce-doped ZnO nanorods with applications in optoelectronic devices.

Raman scattering is very sensitive to the microstructure of nano-sized materials and can be used to obtain the additional information for the Ce-doped ZnO nanorods. Fig. 5 shows the room-temperature Raman spectra of ZnO and Ce-doped ZnO excited by the 514.5 nm line of an argon laser, taken in the backscattering geometry. Wurtzite-type ZnO belongs to the $C_{6v}^4$ ($P63mc$) space group. The zone-center optical phonons can be

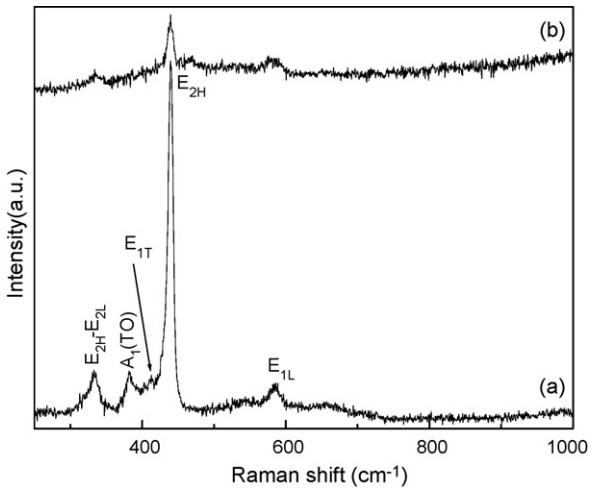


**Fig. 5.** Raman spectra of undoped ZnO nanorods prepared at 900 °C (a) and prepared with Ce-doping nanorods at 500 °C (b).

classified according to the following irreducible representations: $\Gamma_{opt} = A_1 + E_1 + 2E_2 + 2B_1$. The $B_1$ modes are silent modes, the $A_1$ and $E_1$ modes are polar modes and both Raman and infrared active, and they split into transverse optical (TO) and longitudinal optical (LO) phonons, whereas the $E_2$ modes are nonpolar and Raman active only. We observed two peaks located at about 439 and 333 $cm^{-1}$ for both samples which was corresponding to $E_{2H}$ modes and $E_{2H} - E_{2L}$ modes, respectively. Compared with pure ZnO nanorods, the $E_{2H}$ modes of the doped ZnO nanorods blue shift from 441 to 439 $cm^{-1}$, and its intensities decreased. The blue shift is believed to originate from the residual stress along the *c* axis due to the lattice distortion [29]. According to Fig. 3, the $E_{2H}$ peak shows a dominant intensity over the LO phonon peak and a very sharp feature. It indicates that the wurtzite structure formed, pure ZnO and Ce-doped ZnO crystal quality is good, which is in agreement with XRD result. The $E_{1L}$ peak centered at 580 $cm^{-1}$ is considered due to the formation of the defects such as oxygen vacancy and Zn interstitial [21], and this vibration peak is almost invisible in Ce-doped ZnO nanorods, this trend is consistent with the PL result.

## 4. Conclusion

In conclusion, ZnO and Ce-doped ZnO nanorods were controlled achieved via sol–gel method. The PL spectra of Ce-doped ZnO showed a strong UV emission band located at 377 nm and a weak visible emission. More electrons can be contributed by cerium dopants so that the radiative recombination of these excess excitons will lead to a blue shift and broaden of UV emission peak. Raman peaks confirmed Ce-doped nanorods retain their high crystal quality. The facile, reproducible, and effective route presented here provides a useful method for the $RE^{3+}$-doped ZnO system. The high crystal quality of the Ce-doped nanorods and good optical properties under room temperature make it a candidate of optical materials for the applications in the future.

## Acknowledgements

This work is supported by the National Natural Science Foundation of China (Grant No. 60778040), The Ministry of Science and Technology of China (863) (Item No. 2007AA032400448), The Science and Technology Bureau of Jilin Province (Item No. 20060518), Gifted Youth Program of Jilin province (No. 20060123) and The Science and Technology Bureau of Key Program for Ministry of Education (Item No. 207025).

## References


[1] M.H. Huang, S. Mao, H. Feick, H. Yan, Y. Wu, H. Kind, E. Weber, R. Russo, P. Yang, Science 292 (2001) 1897–1899.
[2] W.I. Park, D.H. Kim, S.W. Jung, G.C. Yi, Appl. Phys. Lett. 80 (22) (2002) 4232–4234.
[3] W.I. Park, G.C. Yi, M. Kim, S.J. Pennycook, Adv. Mater. 15 (6) (2003) 526–529.
[4] H. Kind, H.Q. Yan, B. Messer, M. Law, P. Yang, Adv. Mater. 14 (2) (2002) 158.
[5] W.I. Park, G.C. Yi, J.W. Kim, S.M. Park, Appl. Phys. Lett. 82 (4) (2003) 4358–4360.
[6] W.I. Park, G.C. Yi, Adv. Mater. 16 (1) (2004) 87.
[7] S.Y. Bae, C.W. Na, J.H. Kang, J.H. Park, J. Phys. Chem. 1099 (7) (2005) 2526–2531.
[8] S. Gao, H. Zhang, R. Deng, X. Wang, D. Sun, G. Zheng, Appl. Phys. Lett. 89 (12) (2006) 123125–123127.
[9] X.M. Teng, H.T. Fan, S.S. Pan, C. Ye, G.H. Lia, J. Appl. Phys. 100 (5) (2006) 053507.
[10] R. Perez-Casero, A. Gutierrez-Llorente, O. Pons-Y-Moll, J. Appl. Phys. 97 (5) (2005) 054905.
[11] E. Rita, E. Alves, U. Wahl, J.G. Correia, A.J. Neves, M.J. Soares, T. Monteiro, Physica B 340 (2003) 235–239.
[12] B. Cheng, Y. Xiao, G. Wu, L. Zhang, Appl. Phys. Lett. 84 (3) (2004) 416–418.
[13] Z. Bofiani, B. Derkowska, P. Dalasinski, M. Wojdyla, S. Dabos-Seignon, M. Alaoui Lamrani, L. Dghoughi, W. Bala, M. Addou, B. Sahraoui, Opt. Commun. 267 (2) (2006) 433–439.
[14] R. Brundle, R.L. Bickley, J. Chem. Soc., Faraday Trans. II 75 (2) (1979) 1030–1046.
[15] P. Zu, Z.K. Tang, G.K.L. Wong, M. Kawasaki, A. Ohtomo, H. Koinuma, Y. Segawa, Solid State Commun. 103 (1997) 459.
[16] D.M. Bagnall, Y.F. Chen, M.Y. Shen, Z. Zhu, T. Goto, T. Yao, J. Cryst. Growth 184–185 (1998) 605–609.
[17] W. Li, D. Mao, F. Zhang, X. Wang, X. Liu, S. Zou, Y. Zhu, Q. Li, J. Xu, Nucl. Instrum. Methods Phys. Res. B 169 (1–4) (2000) 59–63.
[18] K. Vanheusden, W.L. Warren, C.H. Seager, D.R. Tallant, J.A. Voigt, B.E. Gnade, J. Appl. Phys. 79 (10) (1996) 7983.
[19] Y.W. Chen, Y.C. Liu, S.X. Lu, C.S. Xu, C.L. Shao, C. Wang, J.Y. Zhang, Y.M. Lu, D.Z. Shen, X.W. Fan, J. Chem. Phys. 123 (13) (2005) 134701.
[20] S.H. Jeong, J.K. Kim, B.T. Lee, J. Phys. D 36 (16) (2003) 2017–2020.
[21] L.V. Azaroff, Introduction to Solids, McGraw-Hill, 1960, pp. 371.
[22] K. Vanheusden, C.H. Seager, W.L. Warren, D.R. Tallant, J.A. Voiget, Appl. Phys. Lett. 68 (3) (1996) 403.
[23] G.Z. Shen, J.H. Cho, C.J. Lee, Chem. Phys. Lett. 401 (4–6) (2005) 414–419.
[24] W.S. Shi, O. Agyeman, C.N. Xu, J. Appl. Phys. 91 (9) (2002) 5640–5644.
[25] G.D. Mahan, J. Appl. Phys. 54 (7) (1983) 3825.
[26] K. Hoffmann, D. Hahn, Phys. Stat. Sol. A 24 (2) (1974) 637–648.
[27] B. Cheng, Y. Xiao, G. Wu, L. Zhang, Adv. Funct. Mater. 14 (9) (2004) 913–919.
[28] U. Veaceslav, R. Emil, Z. Victor, S. Lilian, M. Eduard, T. Ion, Inform. Technol. 5822 (2005) 148–155.
[29] S.K. Sharma, G.J. Exarhos, Solid State Phenom. 55 (1997) 32.